

Crystal and electronic structures of Cr_3O_8 and LiCr_3O_8 : Probable cathode materials in Li batteries

R. Vidya,* P. Ravindran, A. Kjekshus, and H. Fjellvåg

Department of Chemistry, University of Oslo, Box 1033 Blindern, N-0315 Oslo, Norway

(Received 29 June 2005; revised manuscript received 3 January 2006; published 16 June 2006)

Ground-state crystal structures are predicted for Cr_3O_8 and LiCr_3O_8 from accurate first-principles density-functional calculations by considering several (25 for the former and 12 for the latter phase) related structure types. Both phases stabilize in monoclinic ($C2/m$) structures with slight variations in the atomic arrangement of the chromium-oxygen framework. Structural optimization is also performed for Cr_8O_{21} , the obtained structural parameters being in good agreement with the experimental values. A possible synthesis route for Cr_3O_8 is suggested from total energy studies. Electronic structure studies indicate insulating behavior with very small band gaps for Cr_8O_{21} and LiCr_3O_8 whereas Cr_3O_8 has pseudogaplike feature. Magnetic property and partial density of states analyses indicate two different valence states for Cr in all studied phases (except CrO_3). Bonding characteristics and effects of Li intercalation in Cr_3O_8 are also analyzed with the help of charge density and charge transfer plots.

DOI: [10.1103/PhysRevB.73.235113](https://doi.org/10.1103/PhysRevB.73.235113)

PACS number(s): 71.20.-b, 75.50.Ee, 82.45.Fk

I. INTRODUCTION

Oxides containing mixed-valent transition metals have attracted much attention since the discovery of colossal magnetoresistance phenomena. The present authors have previously reported¹ on the electronic and magnetic properties of ACr_3O_8 ($A=\text{Na}, \text{K}, \text{Rb}$) which formally contains Cr in mixed-valence states. In this communication we present the results of first-principles density-functional theory (DFT) calculations on the related phases Cr_3O_8 and LiCr_3O_8 . In addition to the mixed-valence aspects associated with chromium, these phases are also of considerable interest in relation to application as cathode material in batteries (see Ref. 2 and references therein).

Rechargeable lithium batteries are attractive for use in light-weight, high-energy-density-storage devices with applications ranging from small portable electronics to larger mobile electrical units. Batteries consist of an anode and a cathode separated by a suitable electrolyte. In lithium batteries, the anode comprises Li at a high chemical potential, e.g., Li metal, Li-Al alloys, or Li dissolved in carbon. A low Li chemical potential is established at the cathode which may have its chemical anchoring in a suitable metal oxide or sulfide that can intercalate Li. Li ions are intercalated into the cathode when the battery is discharged and deintercalated when it is charged. The open cell voltage of the battery is directly proportional to the chemical potential difference between the Li in anode and cathode.³ An appreciable amount of research has been made to find possible Li cathode materials based on lithium-intercalated transition-metal oxides since these materials generally appear to exhibit quite high cell voltages and the series Li_xMO_2 ($M=\text{Ti}-\text{Zn}$) has, e.g., been subjected to a number of first-principles theoretical studies.³⁻⁵

The insertion of Li in chromium oxides by both chemical and electrochemical means was apparently first demonstrated by Koksang and Norby.⁶ Chromium oxides as constituents for cathodes are particularly attractive because of their high energy density and high capacity at low discharge rates. For

example, the calculated energy density for the couple $\text{Li}/\text{Cr}_3\text{O}_8$ is reported to be about twice that of the couple Li/TiS_2 .⁷ Moreover, the couple $\text{Li}/\text{Cr}_3\text{O}_8$ has open circuit and averaged discharge voltages of 3.8 and 3.0 V, respectively, as well as a cell voltage comparable to that of already commercially available lithium batteries. Several studies (see Refs. 2 and 8) have shown that Cr_3O_8 cathodes exhibit good performance for the reversible cycling which involve Li intercalation/deintercalation, and the high energy density and good rechargeability have indeed made it a promising cathode material for Li batteries. It may be mentioned that the maximum charge transfer estimated⁸ for the $\text{Li}/\text{Cr}_3\text{O}_8$ couple is more than 50% larger than the average charge transfer accepted for the batteries developed by the Varta company.⁹ At room temperature Cr_3O_8 (as well as CrO_3 and Cr_8O_{21} which will enter in the consideration below) is insensitive to overdischarging and can be cycled even at voltages of 2 V.¹⁰ A disadvantage which the $\text{Li}/\text{Cr}_3\text{O}_8$ couple has in common with other battery constructions based on intercalation mechanisms is slow kinetics.

In general, the suitability of different host matrices as secondary intercalation cathodes in lithium cells depends on their crystal structure and electronic properties.¹¹ Further the Li ions mobility is mainly related to the atomic architecture of the host structure and more specifically to the electrostatic interaction between Li ions and relevant parts of the host. The maximum lithium uptake is related to the number of sites that can accommodate Li and/or to the number of electronic states available for the corresponding electrons. High Li^+ uptake is clearly beneficial for high energy density, but may be accompanied by serious structural changes of the host. In fact, the interior structure and external morphology of the host may in general suffer appreciably during the intercalation and deintercalation reactions. For example, the repeated cycling of $\text{Li}/\text{Cr}_3\text{O}_8$ cathodes under battery conditions is reported¹² to give rise to increasingly disordered materials (viz. gradual deterioration toward an amorphous state²).

In this scenario, it is likely that structural studies on Cr_3O_8 and LiCr_3O_8 can provide crucial information for the under-

standing of the structural stability and other physical properties of these materials and in turn lead ways to improve their battery performance. However, experimental structural studies on Cr_3O_8 and LiCr_3O_8 are hitherto rather limited,¹³⁻¹⁶ which may be due to difficulties involved in preparation of single crystals. Hence we have undertaken a detailed study on structural stability, electronic structure, magnetic structure, and bonding characteristics for these materials using accurate DFT calculations. The advantage of *ab initio* calculations is that we require only the atomic numbers of the constituents of the phase under investigation and suitable guess structures.

II. COMPUTATIONAL DETAILS

The main aim of the present work has been to establish the ground-state crystal structures of Cr_3O_8 and LiCr_3O_8 , and for this purpose a number of possible guess structures have been considered in the structural optimization calculations using the projected augmented plane-wave¹⁷ (PAW) method as implemented in the Vienna *ab initio* simulation package (VASP).¹⁸ In this approach the valence orbitals are expanded as plane waves and the interactions between the core and valence electrons are described by pseudopotentials. The optimization of the atomic geometry was performed via a conjugate-gradient minimization of the total energy, using Hellmann-Feynman forces on the atoms and the stresses in the unit cell. During the simulations, atomic coordinates and axial ratios are allowed to relax for different volumes of the unit cell. These parameters are changed iteratively so that the sum of the lattice energy and the electronic free energy converges to a minimum value. The ground state is calculated exactly for each set of atomic positions and the electronic free energy is taken as the quantity to be minimized. Convergence minimum with respect to atomic shifts was assumed to have been attained when the energy difference between two successive iterations was less than 10^{-7} eV per unit cell and the forces acting on the atoms were less than $1 \text{ meV } \text{\AA}^{-1}$. The generalized-gradient approximation¹⁹ (GGA) was used to obtain the accurate exchange and correlation energy for all the atomic configurations. The calculations were carried out using $4 \times 8 \times 8$ Monkhorst-Pack \mathbf{k} -points grid, equivalent to 64 \mathbf{k} points in the irreducible Brillouin zone. Any further increase in the number of \mathbf{k} points proved to have negligible effect on the total energy. A plane-wave energy cutoff of 550 eV was used in all calculations. In order to avoid ambiguities in the free-energy results we have used same energy cutoff and \mathbf{k} -point density in all calculations. Calculations were performed for paramagnetic (P), ferromagnetic (F), and antiferromagnetic (AF) configurations of all guess structures with favorably low total energy (notably CrO_3 , Cr_3O_8 -I and -II, Cr_8O_{21} , and LiCr_3O_8 -I and -II). We have calculated the total energy of the compounds as a function of volume for ten different volumes, fitted the results to the so-called “universal equation of state,”²⁰ and extracted the bulk modulus (B_0).

III. STRUCTURAL CONSIDERATIONS

The first structural study¹⁵ of Cr_3O_8 indexed the x-ray diffraction pattern of a sample with the said (not docu-

mented) composition on the basis of an orthorhombic unit cell, with unspecified space group and without any information on atomic positions. The most recent study¹⁶ was performed on a sample with the slightly different composition Cr_8O_{21} and describes the structure as triclinic ($P\bar{1}$) on the basis of information from powder diffraction using conventional x-ray, neutron, and x-ray synchrotron radiation. (The fact that the unit-cell volume reported in Ref. 15 is related to that in Ref. 16 by a factor of nearly four suggests that the sample of the former study in reality may have consisted of Cr_8O_{21} .) According to Norby *et al.*¹⁶ the Cr_8O_{21} structure consists of $\text{Cr}^{\text{III}}\text{O}_6$ octahedra and $\text{Cr}^{\text{VI}}\text{O}_4$ tetrahedra. These polyhedra form sheets which are held together by tetrachromate Cr_4O_{13} groups to form a three-dimensional framework [Fig. 1(d)].

Despite the difference in composition, the Cr_8O_{21} structure was an obvious choice of guess structure for the structural optimization calculations. Two other equally obvious choices were the oxide segments (designated Cr_3O_8 -I and -II) that remain after stripping off K from the KCr_3O_8 -type^{1,21,22} structure [Fig. 1(b); space group $C2/m$], and Li from the LiCr_3O_8 structure [Fig. 1(c); space group $Cmcm$ with random distribution of the Li atoms and one third of the Cr atoms¹³] and also the oxide framework of other structures considered for the optimization of LiCr_3O_8 (see below). Similarly we considered a guess structure based on a modified²³ Hf_3O_8 ($P2_1/m$) arrangement in which H is omitted and I is replaced by Cr. In order to have larger platform for the exploration of the ground state structure of Cr_3O_8 , we extended the selection of guess structures to other alternatives with 3:8 stoichiometry, being perfectly aware that some of these are rather unlikely for an oxide such as Cr_3O_8 . We considered the structure types²³ of the following reasonably related compounds as inputs in the structural optimization calculations: Nb_3Cl_8 ($P\bar{3}m1$), Rh_3Se_8 ($R\bar{3}$), $\alpha\text{-W}_3\text{O}_8$ ($C222$), $\beta\text{-W}_3\text{O}_8$ ($Pbam$), Ir_3Se_8 ($R\bar{3}$), $\alpha\text{-U}_3\text{O}_8$ ($P\bar{6}2m$), $\beta\text{-U}_3\text{O}_8$ ($Cmcm$), $\gamma\text{-U}_3\text{O}_8$ ($P2_1/m$), $\delta\text{-U}_3\text{O}_8$ ($P\bar{3}$), and $\epsilon\text{-U}_3\text{O}_8$ ($Amm2$). In the course of the study it also seemed appropriate to perform structural optimization on²⁴ CrO_3 which comprises a virtually one-dimensional arrangement of strings of corner sharing CrO_4 tetrahedra [Fig. 1(a)].

We considered also a number of different structure types as inputs to establish the ground-state structure of LiCr_3O_8 . Obviously one starting point had to be the experimentally reported¹³ LiCr_3O_8 structure based on $Cmcm$ symmetry. This structure is described as built up of somewhat staggered strings of (Li,Cr) O_6 octahedra connected by edge sharing in the c direction, the strings being in turn linked via corner-sharing CrO_4 tetrahedra to give the structure a certain three-dimensional character. The present simulations of the LiCr_3O_8 structure [Fig. 1(f); designated LiCr_3O_8 -II] were performed in a supercell which also took care of the cooperative magnetic order. Another atomic arrangement which had to come on top of the priority list was the KCr_3O_8 -type structure [Fig. 1(e); space group $C2/m$ with K exchanged by Li; designated LiCr_3O_8 -I] which is adopted by the succeeding elements $A = \text{Na}, \text{K}, \text{Rb}$ in the $A\text{Cr}_3\text{O}_8$ series.^{1,21,22} In addition to these structure types, the following variants²³

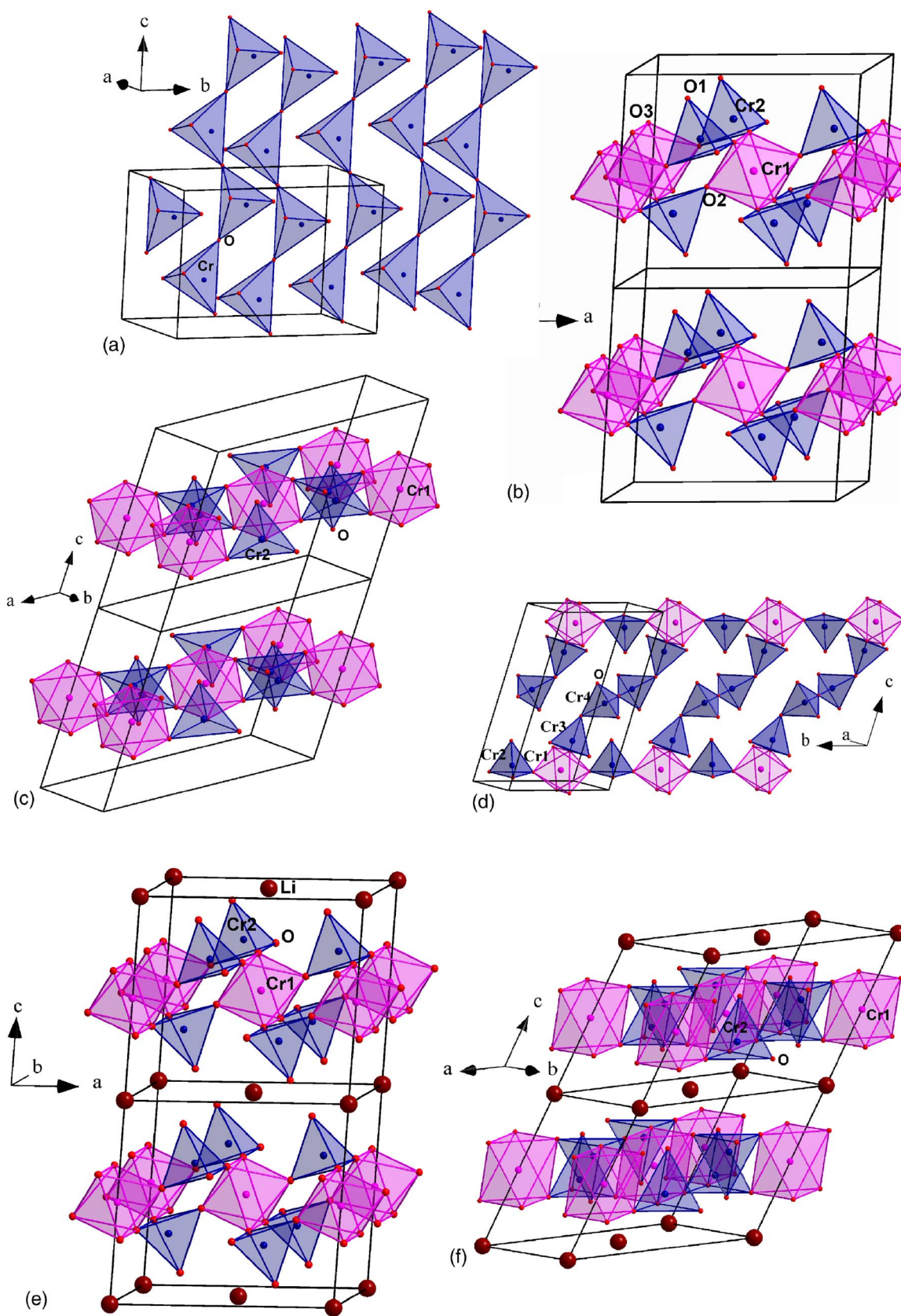


FIG. 1. (Color online) Crystal structure of (a) CrO_3 ($Ama2$), (b) $\text{Cr}_3\text{O}_8\text{-I}$ ($C2/m$), (c) $\text{Cr}_3\text{O}_8\text{-II}$ ($C2/m$), (d) Cr_8O_{21} ($P\bar{1}$), (e) $\text{LiCr}_3\text{O}_8\text{-I}$ ($C2/m$), and (f) $\text{LiCr}_3\text{O}_8\text{-II}$ ($C2/m$). Crystallographically different chromium atoms are labeled on the illustrations. Tetrahedral and octahedral Cr-O polyhedra are distinguished by different shading (color).

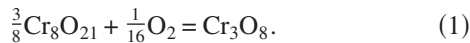
were considered: HI_3O_8 ($P2_1/m$; Li at the H site, and Cr at the I site), LiV_3O_8 ($P2_1/m$), LiNb_3O_8 ($P2_1/c$), α - LiTa_3O_8 ($C2/c$), β - LiTa_3O_8 ($Pmma$), α - NaNb_3O_8 ($Ibam$), β - NaNb_3O_8 ($Pba2$), KNb_3O_8 ($Cmcm$), ZnV_3O_8 ($Iba2$), CuNb_3O_8 ($P2_1/c$), $\text{AgBiCr}_2\text{O}_8$ ($I\bar{4}$), TlV_3O_8 ($P2_1/m$), and CsCr_3O_8 ($Pnma$).

IV. RESULTS AND DISCUSSION

A. Structural aspects

Among the different test-structural arrangements considered for chromium oxides with 3:8 stoichiometry, that derived by omitting K from the KCr_3O_8 -type structure (viz. Cr_3O_8 -I; in AF state) came out with the lowest calculated total energy [see Fig. 2(a) and Table I for structure specifications]. Other variants with the 3:8 stoichiometry came out with moderate [e.g., LiV_3O_8 type minus Li; $\Delta E=0.43$ eV per Cr_3O_8 unit] to much higher total energies [e.g., Ir_3O_8 type; $\Delta E=7.52$ eV per Cr_3O_8 unit]. A particular relevant test structure for comparison with the ground-state Cr_3O_8 -I variant is Cr_3O_8 -II derived by omitting Li from LiCr_3O_8 -II [see below and Figs. 1(e) and 2(c)]. As seen from Fig. 2(a) Cr_3O_8 -II exhibits an appreciably higher energy than Cr_3O_8 -I, in fact, Cr_3O_8 -II is located well above the mentioned Li-stripped-off variant of the LiV_3O_8 -type structure.

The experimentally established Cr_8O_{21} phase, on the other hand, takes a slightly different composition and an appreciably different structural arrangement from Cr_3O_8 -I [see Figs. 1(b) and 1(c)]. The total energy (E) vs unit-cell volume (V) relationship for Cr_8O_{21} [Fig. 2(b)] shows nearly the same ground-state energy ($E=-85.83$ eV per $\text{Cr}_3\text{O}_{7.875}$) as Cr_3O_8 -I ($E=-86.06$ eV per Cr_3O_8) whereas the corresponding cell volumes differ appreciably ($V=163.25 \text{ \AA}^3$ per $\text{Cr}_3\text{O}_{7.875}$ and 139.01 \AA^3 per Cr_3O_8). However, a proper comparison between Cr_8O_{21} and Cr_3O_8 has to take into account the difference in oxygen content as brought out by the reaction equation

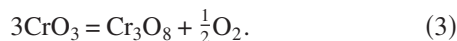


The oxidation energy (ΔE) follows from the relation:

$$\Delta E = E(\text{Cr}_3\text{O}_8) - \frac{3}{8}E(\text{Cr}_8\text{O}_{21}) - \frac{1}{16}E(\text{O}_2), \quad (2)$$

which upon introduction of the calculated values for Cr_3O_8 , Cr_8O_{21} , and the dioxygen molecule ($E=-9.8607$ eV) gives $\Delta E=-0.39$ eV per Cr_3O_8 at 0 K. This confirms that the experimentally established Cr_8O_{21} phase is the real ground-state phase for the oxide in question. However, as will be argued below there are reasons to believe that Cr_3O_8 -I can be obtained as a metastable phase under electrochemical conditions.

So far all attempts^{2,6,8,12-16} to synthesize Cr_3O_8 have made use of thermal decomposition of CrO_3 as a key element in the preparational procedure



According to the present total energy data (see Fig. 2) Cr_3O_8 should be obtainable according to Eq. (3) already at

0 K ($\Delta E=-5.20$ eV per Cr_3O_8 or -1.73 eV per $\text{CrO}_{2.667}$). However, formation of Cr_8O_{21} should be even more favorable ($\Delta E=-1.86$ eV per $\text{CrO}_{2.625}$). We will return to a possible synthesis route to Cr_3O_8 after the presentation of our findings for LiCr_3O_8 . It should be noted that our attempts to perform DFT structural optimization for CrO_3 proved rather unsuccessful. In the first place the calculations converged rather slowly and oscillating, and also they terminated at unit-cell dimensions and positional parameters much different from the experimental values.²⁴ We believe that the root of the problem is the distinct one-dimensional character of the CrO_3 structure which may obscure the DFT calculation. It is well known that the DFT approach (in particular GGA) underestimates intermolecular, van der Waals-type binding.

As seen from Fig. 2(c), two of the selected test structures for LiCr_3O_8 (variants I and II) came out with virtually the same total energy at the minimum in the $E(V)$ relationship ($\Delta E \approx -5.6$ meV per LiCr_3O_8) with variant II as the energetically favored phase. Variant II has also the smallest equilibrium volume ($V=143.19$ and 148.44 \AA^3 per $\text{Li}_3\text{Cr}_3\text{O}_8$ for variant II and I, respectively). As seen from Table I, both LiCr_3O_8 -I and -II belong to the space group $C2/m$, even though the initial guess structures were different. We simply allotted the KCr_3O_8 type to variant I and the experimentally determined LiCr_3O_8 structure to variant II. According to Wilhelmi's¹³ description for the LiCr_3O_8 -II structure in space group $Cmcm$, Li and one third of the Cr atoms are randomly distributed in a fourfold position. In order to bring the disorder aspect into the computations, we constructed a supercell with periodic arrangements of Li and Cr1 to mimic the experimentally reported structure. At the start of the calculations it was detected that forces of around 2.6 eV \AA^{-1} were acting at the oxygen sites which clearly signaled certain defects in the experimental LiCr_3O_8 -II structure. This suspicion was further reinforced during the calculations which finally converged with a gain of more than 1.3 eV f.u.^{-1} in total energy and structural parameters that were "miles away" from the input values. On careful analysis of our computed LiCr_3O_8 -II structure it turned out that this really belongs to space group $C2/m$ rather than $Cmcm$. Although this is "accidentally" the same space group as adopted by variant I, the atomic arrangement is quite different. With our retrospective wisdom we tried to convert Wilhelmi's structure to space group $C2/m$, but the efforts were in vain. Hence the calculated structure specification included in Table I represents an appreciably modified version of Wilhelmi's structure, and it is pertinent to ask what can possibly have gone wrong in Wilhelmi's single-crystal x-ray determination of the LiCr_3O_8 -II structure. We believe that the root of the discrepancy is associated with the chemically rather unrealistic postulate that Li and Cr atoms should be randomly distributed over one and the same site in such structures. On the basis of the present theoretical findings it is strongly recommended that the LiCr_3O_8 -II structure is subjected to an experimental redetermination.

From Figs. 1(e) and 1(f) it is seen that LiCr_3O_8 -I and -II carry a close structural relationship, both exhibiting characteristic layer features. Wilhelmi¹³ used relatively strong syntheses means (hydrothermal conditions at high temperatures) to obtain the LiCr_3O_8 -II phase. On modifying the

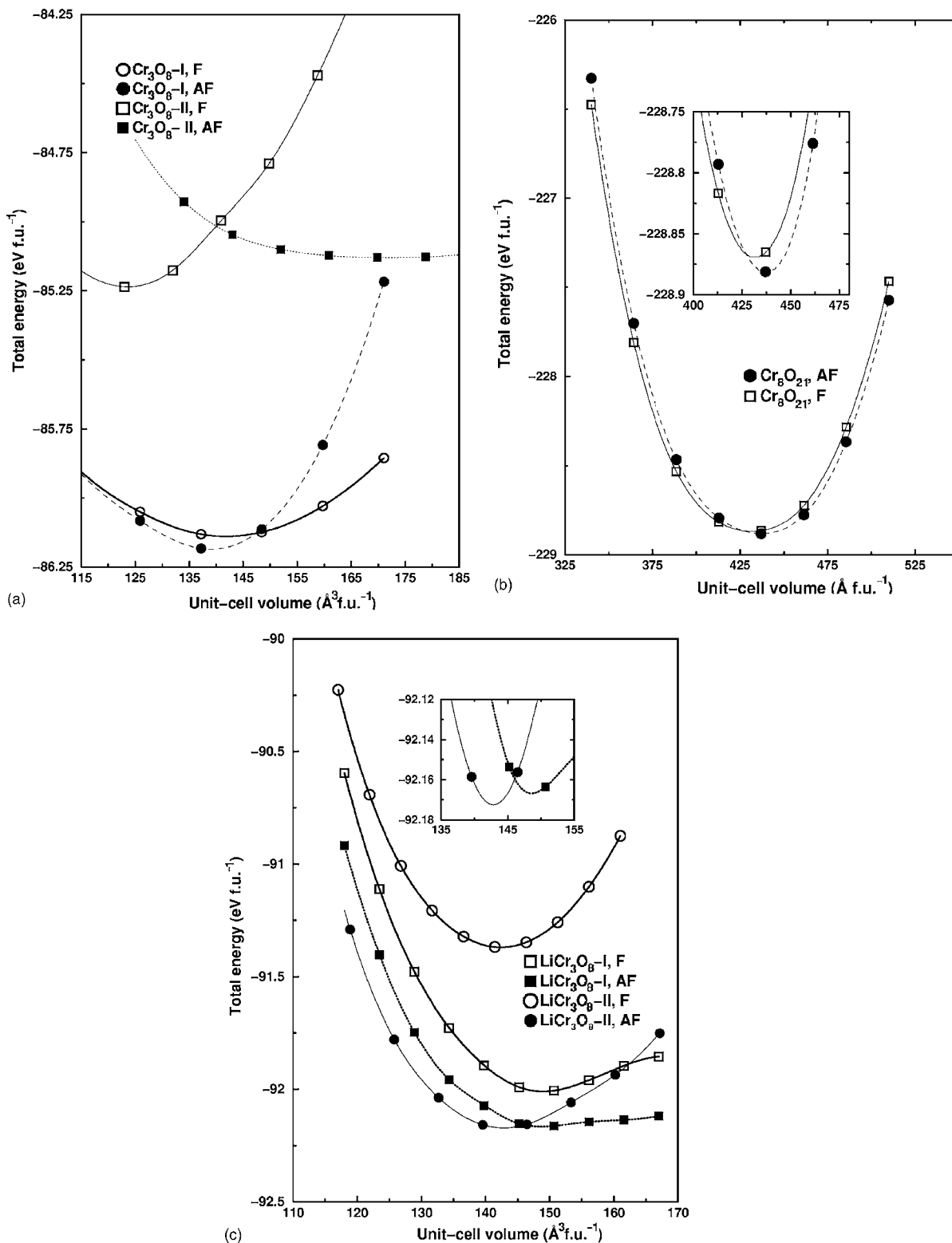


FIG. 2. Calculated unit-cell volume vs total energy for (a) Cr₃O₈-I and -II, (b) Cr₈O₂₁, and (c) LiCr₃O₈-I and -II in ferro- and antiferromagnetic configuration. See Fig. 1 and Table I for structural information.

preparational procedure (among other things, relinquishing single-crystal production) and rather imitating the synthesis procedures for the other ACr₃O₈ (A=Na,K,Rb) phases²² it seems quite likely that the LiCr₃O₈-I phase will materialize. With the LiCr₃O₈-I phase at hand, it is easy to prescribe an

apparently safe synthesis route to Cr₃O₈-I. LiCr₃O₈-I is simply introduced as cathode in a suitable battery setup and the unit is subjected to charging conditions.

The structural feature which makes the LiCr₃O₈-I phase particularly suitable for battery purposes is its pronounced

TABLE I. Optimized structure parameters and bulk modulus (B_0) for Cr_3O_8 -I, and -II, Cr_8O_{21} and LiCr_3O_8 -I and -II. All structures, except Cr_8O_{21} ($P\bar{1}$), are described in space group $C2/m$ with Li in $2a$ and Cr1 in $2c$ (not included in the listing). Values given in parentheses refer to the experimental data for Cr_8O_{21} (Ref. 16). For comments about the experimental data for LiCr_3O_8 -II (Ref. 13), see text.

Compound	Unit cell (Å or deg)	Atom	Site	x	y	z	B_0 (GPa)
Cr_3O_8 -I	$a=8.4067$	Cr2	$4i$	0.5528	0	0.2598	34.743
	$b=5.2656$	O1	$4i$	0.2007	0	0.5884	
	$c=6.0462$	O2	$4i$	0.2971	0	0.9770	
	$\beta=91.03$	O3	$8j$	0.0495	0.2433	0.3083	
Cr_3O_8 -II	$a=6.7524$	Cr2	$4i$	0.3675	0	0.5930	4.396
	$b=5.6422$	O1	$4i$	0.2205	0	0.6579	
	$c=7.7150$	O2	$4i$	0.7184	0	0.6399	
	$\beta=117.85$	O3	$8j$	0.9769	0.2460	0.6595	
Cr_8O_{21}	$a=5.434$ (5.433)	Cr1	$2i$	0.852 (0.859)	0.211 (0.211)	0.069 (0.068)	21.424
	$b=6.637$ (6.557)	Cr2	$2i$	0.296 (0.280)	0.235 (0.234)	0.899 (0.898)	
	$c=12.546$ (12.117)	Cr3	$2i$	0.347 (0.358)	0.368 (0.377)	0.248 (0.258)	
	$\alpha=105.86$ (106.36)	Cr4	$2i$	0.731 (0.721)	0.793 (0.799)	0.529 (0.528)	
	$\beta=95.36$ (95.73)	O1	$2i$	0.813 (0.800)	0.500 (0.504)	0.066 (0.060)	
	$\gamma=77.70$ (77.96)	O2	$2i$	0.423 (0.426)	0.817 (0.835)	0.036 (0.049)	
		O3	$1f$	$1/2$ ($1/2$)	0 (0)	$1/2$ ($1/2$)	
		O4	$2i$	0.132 (0.127)	0.238 (0.250)	0.173 (0.182)	
		O5	$2i$	0.374 (0.381)	0.725 (0.727)	0.814 (0.812)	
		O6	$2i$	0.329 (0.304)	0.855 (0.859)	0.231 (0.243)	
		O7	$2i$	0.910 (0.911)	0.897 (0.899)	0.055 (0.057)	
	O8	$2i$	0.385 (0.383)	0.328 (0.358)	0.382 (0.397)		
	O9	$2i$	0.026 (0.038)	0.116 (0.115)	0.412 (0.406)		
	O10	$2i$	0.189 (0.183)	0.385 (0.372)	0.583 (0.591)		
	O11	$2i$	0.262 (0.261)	0.617 (0.632)	0.255 (0.255)		
LiCr_3O_8 -I	$a=8.3394$	Cr2	$4i$	0.3570	0	0.2613	49.102
	$b=5.4749$	O1	$4i$	0.2278	0	0.4572	
	$c=6.4185$	O2	$4i$	0.2599	0	0.0425	
	$\beta=90.43$	O3	$8j$	0.4733	0.2575	0.2757	
LiCr_3O_8 -II	$a=9.8811$	Cr2	$4i$	0.3741	0	0.6199	53.522
	$b=5.6842$	O1	$4i$	0.2423	0	0.7135	
	$c=6.1364$	O2	$4i$	0.2329	0	0.6953	
	$\beta=123.91$	O3	$8j$	0.9913	0.2458	0.7248	

layer character (such as monoclinic²⁵ LiMnO_2 where the structure allows withdrawal of large amounts of Li) and the direct correspondence between the structures of Cr_3O_8 -I and LiCr_3O_8 -I [see Figs. 1(b) and 1(e)] which should facilitate lithium intercalation/deintercalation. It is the close structural relationship which will allow preparation of Cr_3O_8 -I as a metastable phase at the expense of the energetically more favorable Cr_8O_{21} (see above). The synthesis of Cr_8O_{21} has been made with use of CrO_3 as starting material and it is indeed possible to imagine that Cr_3O_8 -I as well as Cr_8O_{21} can be formed by reconstructions from structural fragments obtained by partial thermal decomposition of CrO_3 . However, thermal decomposition requires elevated temperature

and under these conditions the energetically favored Cr_8O_{21} is formed. On the other hand, under the far milder electrochemical conditions during deintercalation of LiCr_3O_8 -I, Cr_3O_8 -I should be favored by kinetics. Since the energy barrier between Cr_3O_8 -I and Cr_8O_{21} is higher than the energy made available by room temperature, the activation energy needed to promote the conversion from the former to the latter is simply not available.

Table I shows that Li intercalation from Cr_3O_8 -I to LiCr_3O_8 -I leads to relatively small changes in the a and b axes (-0.8% and 3.1% , respectively) whereas there occurs an appreciable increase in the c axis (6.2%). This nicely illustrates the requirements to a good cathode battery material

based on intercalation/deintercalation mechanisms and emphasizes why the pair Cr₃O₈-I/LiCr₃O₈-I constitutes a good combination. Considerations of the structural information in Fig. 1 and Table I suggest why this pair should be better than other chromium-oxygen combinations: CrO₃ appears to be rather unsuitable for intercalation/deintercalation associated with its one-dimensional structure, Cr₈O₂₁ exhibits too much three-dimensional character, whereas Cr₃O₈-II carries a more irregular arrangement than Cr₃O₈-I. Moreover, most of the cathode materials tested hitherto^{2,8,10,25–28} appear to have contained a mixture of CrO₃, Cr₃O₈ (most likely Cr₈O₂₁ according to the preparational conditions), Cr₅O₁₂, and/or Cr₂O₅, of which CrO₃, Cr₅O₁₂, and Cr₂O₅ as well as the lower oxides CrO₂ and Cr₂O₃ are all reported³ to decrease the performance of lithium chromium oxides as battery materials. Most of the attention has been focused on poorly characterized samples with the composition Cr₃O₈. Since these materials probably consisted of Cr₈O₂₁ it is only natural that the capacity of Li intercalation is found to increase with increasing degree of amorphous character of these samples.⁸ Even with its probable shortcomings (compared to Cr₃O₈-I) unspecified Cr₃O₈ is reported⁸ to exhibit a quite large chemical diffusion coefficient for Li⁺ ($\sim 10^{-8}$ cm² s⁻¹). This appears to vouch for an appreciably higher diffusion of Li⁺ during intercalation/deintercalation of Cr₃O₈-I, which we still regard as a very promising battery cathode material.

B. Magnetic properties

During the structural optimization, we also took into account cooperative magnetic ordering and performed simulations for F, AF, and AF configurations. [Our experience from the calculations of magnetic states for the closely related ACr₃O₈ (A=Na, K, Rb) series showed¹ that tested configurations with ferrimagnetic arrangements invariably ended up with F or AF solutions. Accordingly, such variants were not considered in this study.] As seen from Fig. 2, the AF arrangements came out as the ground states for all phases, except Cr₃O₈-II which takes F ordering as the lower-energy state. The energy difference between the AF and F states is small in all cases (between ~ 4 and 160 meV f.u.⁻¹). These findings suggest that some of the considered phases may be subjected to an AF-to-F transition on application of a magnetic field.

According to Table II one of the Cr sites in all these phases carries a substantial magnetic moment (1.4–2.5 μ_B per Cr atom for the AF states at 0 K and ambient pressure) whereas the other Cr sites only exhibit small moment(s). On considering Table II it should be borne in mind that the oxygen atoms also carry small induced magnetic moments. Some of these turned out to be oppositely aligned in the F cases, hence the total moments for Cr₃O₈-I and -II came out smaller than the sum of the moments at the Cr1 and Cr2 sites.

Experimental magnetic data are very scarce for these phases: limited to $\mu_P = 4.2 \pm 0.1 \mu_B$ per Cr atom, $\Theta = -165 \pm 5$ K, and T_N around 100 K for Cr₈O₂₁,¹⁶ and $\mu_P = 4.35 \mu_B$ per Cr atom, $\Theta = -170$ K, and T_N around 80 K for Cr₃O₈ (unspecified).¹⁵ [Note that these data refer to P states

TABLE II. Calculated magnetic moment (in μ_B per Cr atom) for crystallographically nonequivalent Cr atoms (see Fig. 1 and Table I) for CrO₃, Cr₃O₈-I, Cr₃O₈-II, Cr₈O₂₁, LiCr₃O₈-I, and LiCr₃O₈-II in F and AF states. Total refers to the total magnetic moment per formula unit.

Phase	F			AF	
	Cr1	Cr2	Total	Cr1	Cr2
CrO ₃	1.91		1.87	1.36	
Cr ₃ O ₈ -I	1.78	0.17	1.94	1.67	0.02
Cr ₃ O ₈ -II	1.93	0.18	1.96	1.83	0.05
Cr ₈ O ₂₁	2.39	0.26 ^a	5.61	2.34	0.04 ^b
LiCr ₃ O ₈ -I	2.55	0.22	2.89	2.45	0.02
LiCr ₃ O ₈ -II	2.60	0.22	2.87	2.57	0.04

^aFor Cr3: 0.21 and Cr4: 0.15.

^bFor Cr3: 0.21 and Cr4: 0.02.

with numerical values extracted from Curie-Weiss relationships and thus follow a different definition of magnetic moment; according to the “spin-only” approximation specified as: $\mu_P = \sqrt{8C_{mol}} = 2\sqrt{S(S+1)}$.] However, powder neutron diffraction was only able to unveil a few very weak magnetic reflections at low temperatures (10–100 K) for Cr₈O₂₁.¹⁶ Perhaps the clear indication of Néel temperatures in the magnetic susceptibility data for these phases reflects conversion to two- rather than three-dimensional cooperative magnetic ordering.

The magnetic moments at the Cr1 (Cr for CrO₃) sites in these phases are lower than the spin-only values for a Cr^{III} (d^3) valence state, owing to strong Cr-O interactions (see Sec. IV D). Without our prior experience from the study of the ACr₃O₈ phases we might have at first been tempted to take the observation of very low magnetic moments at the Cr2 sites as indications of a Cr^{VI} (d^0) valence state. (The fact that we then would have overlooked that Cr^{VI} is the formal valence state for CrO₃ is another story.) However, we know¹ that the almost zero moments of Cr2 in the ACr₃O₈ phases do not reflect a d^0 state, but rather result from very small exchange splitting. The large moments at the Cr1 sites, on the other hand, reflect precisely the opposite, viz. strong exchange interaction. The overall size and variation of the magnetic moments in Table II clearly demonstrate that little physical significance should be attached to considerations based on formal valence states (see also Sec. IV D). It is interesting to note that the magnetic moment at Cr1 increases by approximately 1 μ_B from Cr₃O₈-I and -II to LiCr₃O₈-I and -II, respectively. This should not be interpreted as a trivial change in valence state from, say, Cr^{VI} to Cr^{III} but mostly as another evidence for effects of exchange splitting. In this perspective the impacts of differences in the valence states of Cr1 and Cr2 have far less significance.

C. Electronic structure

The total and site-projected DOSs for CrO₃, Cr₈O₂₁, Cr₃O₈-I, and Cr₃O₈-II are displayed in Fig. 3. The total den-

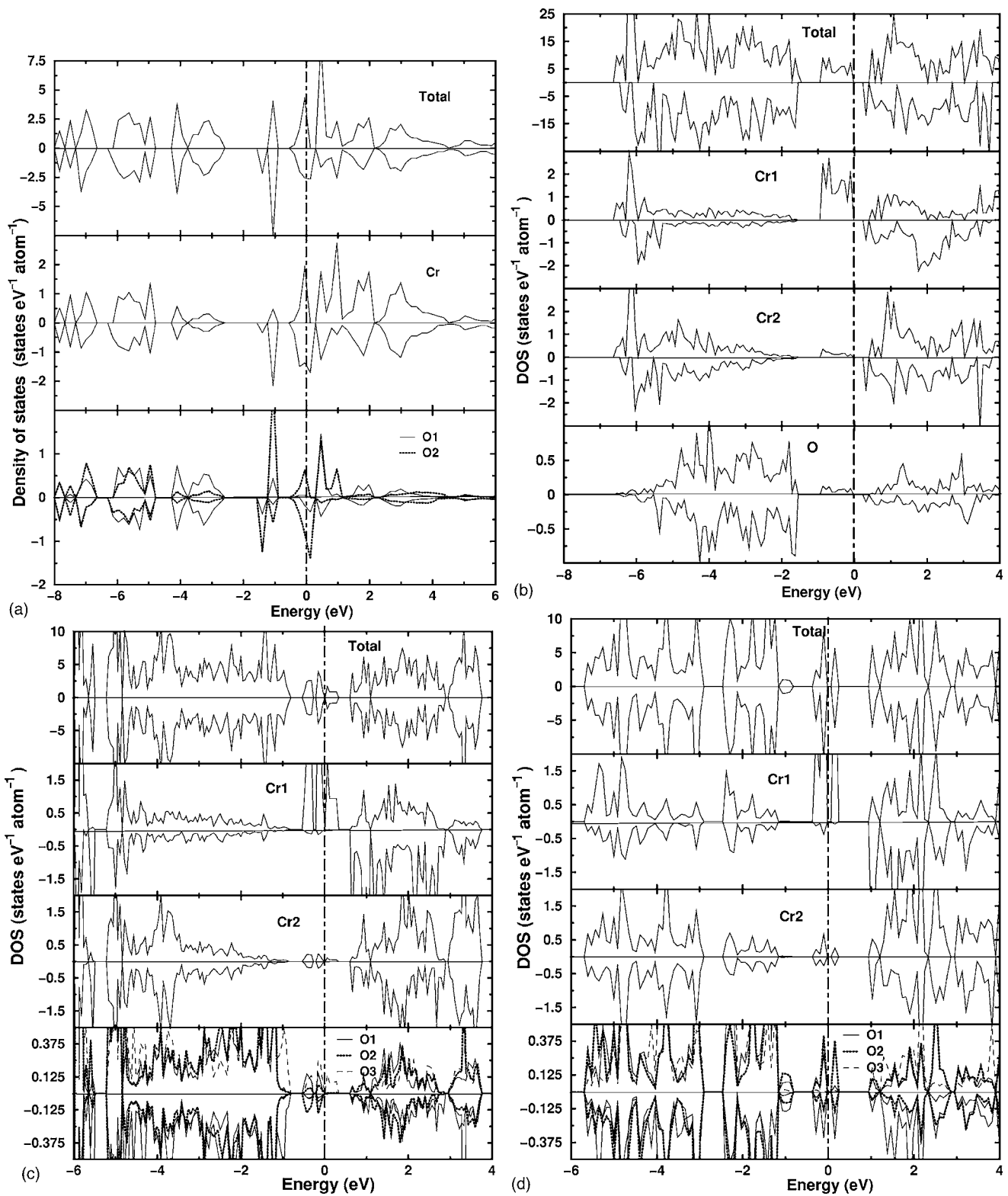


FIG. 3. Total and site-projected density of states for (a) CrO_3 (based on experimental structural parameters), (b) Cr_8O_{21} , (c) Cr_3O_8 -I, and (d) Cr_3O_8 -II; in AF configurations for the three former oxides and F configuration for the latter. The vertical line denotes E_F .

sity of states (DOS) for CrO_3 [Fig. 3(a)] with a significant number of states at the E_F implies metallic character contrary to the insulating behavior expected for a Cr^{VI} state. This confirms that the Cr valence is not in a simple Cr^{VI} state, in agreement with magnetic moment study.

The total DOS for Cr_8O_{21} [Fig. 3(b)] shows insulating behavior with around 0.25 eV band gap between the valence band (VB) and conduction band (CB) which provides another evidence of the relative stability of this oxide compared with Cr_3O_8 -I and -II. Cr_8O_{21} comprises four crystallographi-

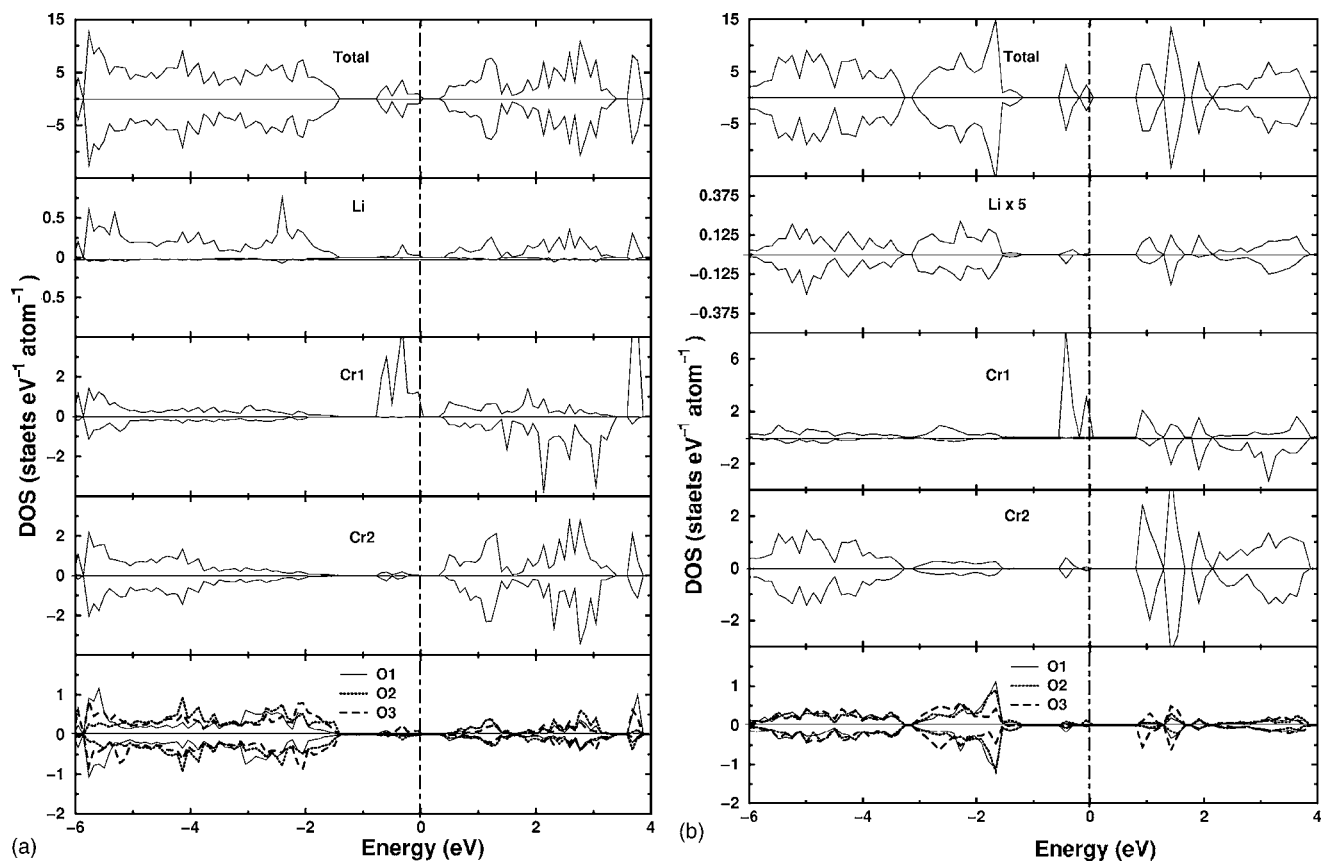


FIG. 4. Total and site-projected density of states for (a) LiCr_3O_8 -I and (b) LiCr_3O_8 -II in AF state. The vertical line denotes E_F .

cally nonequivalent Cr and eight O atoms. Since the energetic distribution of the electronic states for Cr3 and Cr4 are almost same as that for Cr2, illustrations of the site-projected DOS for the former sites are not included in Fig. 3(b). Only an overall DOS is shown for the oxygen atoms of Cr_8O_{21} . The E_F in Cr_3O_8 -I [Fig. 3(c)] falls on a pseudogaplike feature. Pseudogaps are known²⁹ to result from covalent hybridization, exchange splitting, charge transfer, d resonance, etc., and the presence of a pseudogap appears to be favorable for stability. The Cr_3O_8 -II phase, for which both F and AF configurations occur at higher energy than the Cr_3O_8 -I phase [see Fig. 2(a)], exhibits a very small band gap [0.04 eV; Fig. 3(d)] and accordingly insulating behavior at 0 K. The band gap of Cr_8O_{21} is considerably larger lending further support to the conclusion that Cr_8O_{21} is more stable than the two Cr_3O_8 variants, viz. in agreement with findings from the total energy study.

The DOS for the Cr atoms in Cr_3O_8 -I and -II as well as in Cr_8O_{21} show different topology indicating difference in their valence states. The partial DOS of Cr1 in all three phases are similar in the sense that the most prominent peaks are seen in the region -6 to -4 eV and in a narrow region just below the E_F . The majority- and minority-spin channels of Cr2 are almost equally filled, and this implies as mentioned above negligible exchange splitting and consequently a negligible moment at Cr2. More prominent broader densities are seen from -6 to -2 eV in the VB of both Cr1 and Cr2. Cr1 has sharp peaks closer to E_F (from -1 to 0 eV) which can be attributed to the t_{2g} orbitals. The crystal field effect brings

further stability to the system which can be seen from the splitting of the states closer to E_F . On the other hand, Cr2 does not have much DOS close to E_F which implies empty e_g orbitals and hence larger oxidation state for Cr2 than for Cr1. The x-ray photoemission (XPS) study⁸ on Cr_3O_8 samples (unspecified phase) reported two prominent peaks which were interpreted as evidence for the presence of Cr^{6+} and Cr^{3+} ions. Although assignment of valence states is not appropriate using XPS, the site-projected DOS of Cr1 and Cr2 in Figs. 3(b)–3(d) show two such prominent peaks in VB. Owing to the presence of energetically degenerate Cr d and O p states and the layered nature of these phases, the covalent interaction between these atoms is distinct, and indeed it is this interaction which is responsible for the small magnetic moments at the oxygen sites. (See Fig. 3.)

The electronic structures of LiCr_3O_8 -I and -II (Fig. 4) are largely similar. Compared with Cr_3O_8 -I and -II, LiCr_3O_8 -I and -II may be said to have the states more localized. Insulating behavior is seen for both phases with band gaps of around 0.34, and 0.81 eV, respectively. Clearly visible Li states occur in the VB for LiCr_3O_8 -I whereas the Li DOS profile for LiCr_3O_8 -II becomes visible only after appreciable magnification, indicating that Li in LiCr_3O_8 -I is less ionic than that in LiCr_3O_8 -II. Similar to the corresponding Cr_3O_8 -I and -II variants, the two types of Cr atoms in LiCr_3O_8 -I and -II exhibit topologically different partial DOS. The three kinds of oxygen atoms show differences in the DOS curves like those in Cr_3O_8 -I and -II. The partial DOS of Cr and O are energetically degenerate also for the lithium

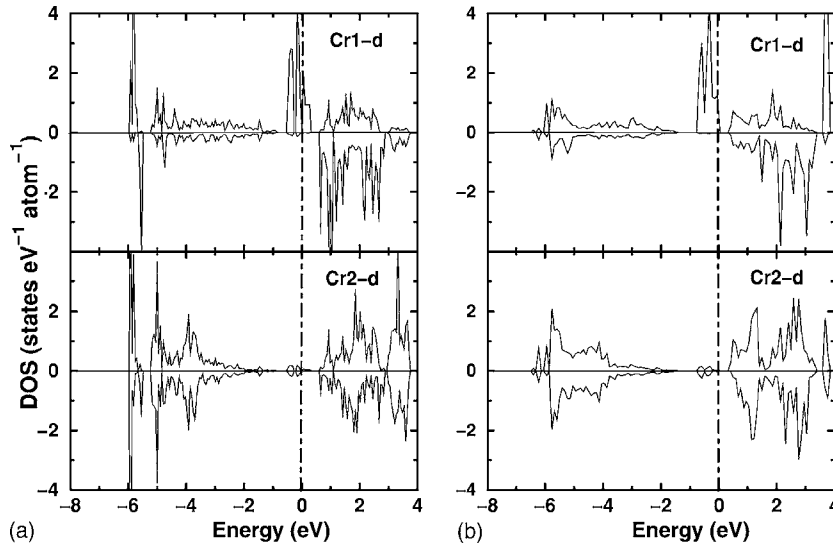


FIG. 5. *d*-orbital-projected density of states for Cr1 and Cr2 of (a) Cr_3O_8 -I and (b) LiCr_3O_8 -I in AF state. The vertical line denotes E_F .

phases (viz. hybridized). As is to be expected on the basis of the close structural correspondence between LiCr_3O_8 -I and -II and the $^1\text{ACr}_3\text{O}_8$ compounds, there are also pronounced similarities in the electronic structures of these phases.

It would be appropriate to recall that formal valence state is an accounting tool for keeping track of electrons engaged in bonding interactions and normally denoted with roman numerals. Oxidation state is reserved for the idealized cases with only pure ionic bonding and denoted with arabic numerals. (In reality oxidation state is also a formal electron accounting tool and mixing up of these two notations often leads to confusion.) Electron accounting according to a pure ionic scheme gives charges of 4+ and 6+ on Cr1 and Cr2, respectively, in Cr_3O_8 . When Li is intercalated into Cr_3O_8 an extra electron, formally donated by Li, goes to Cr1 and changes its charge to 3+. However, the present computations show that, for all compounds, the VB contains a large (roughly equal) number of states for Cr1 and Cr2 (certainly no way near the d^0 configuration required for a Cr^{6+} state). Owing to the hybridization interaction with O 2*p*, the states at the Cr2 site could at first sight seem to originate from back donation. However, the orbital-projected DOS (Fig. 5) for Cr1 and Cr2 in Cr_3O_8 and LiCr_3O_8 demonstrates a definite number of *d* states (integrated counts gave 3 to 5 electrons; *s* and *p* states are negligibly small and not included in the illustrations).

In an effort to find the actual valence states (sum of the estimated number of electrons involved in ionic, covalent,

and metallic bonding interactions according to theory) of Cr atoms, we have attempted to quantify the number of electrons present in a given atomic site. We have calculated the Born effective charges (BEC) for the paramagnetic LiCr_3O_8 -I. The Born effective charges give information about the amount of electrons that are polarized by the application of an electric field.^{30,31} If the atomic species behave such as closed-shell ions, they should carry an effective charge approximately equal to their nominal ionic value. When the lattice is subjected to displacement, a large amount of nonrigid delocalized charge will flow across the skeleton of the lattice with covalent directed bonds. Owing to this covalence effect one usually obtains larger BEC than the nominal ionic values. High Born-effective charge values indicate that the relative displacements of neighboring ions against each other trigger highly polarized electrons. Hence BEC can be considered as an upper limit for the valences in a given system.

The calculated BEC tensor for LiCr_3O_8 -I in paramagnetic (insulator) configuration is given in Table III. One can see that the diagonal components for all constituents are highly anisotropic. The average value of the diagonal components of the BEC tensor for Li, Cr1, Cr2, and O1 are 1.36, 3.54, 4.57, and -1.61 , respectively. The difference in these values for Cr1 and Cr2 clearly indicate the difference in their valence states; even though Cr1 can be assigned Cr^{III} , Cr2 cannot be assigned a Cr^{VI} state. The higher than nominal ionic values for the effective charges and the non-negligible off-

TABLE III. Calculated Born effective charge tensor (Z_{ij}^*) for nonmagnetic LiCr_3O_8 -I.

Species	Z_{xx}^*	Z_{yy}^*	Z_{zz}^*	Z_{xy}^*	Z_{xz}^*	Z_{yx}^*	Z_{yz}^*	Z_{zx}^*	Z_{zy}^*
Li	1.85	1.51	0.73	0.00	-0.22	0.00	0.00	0.01	0.00
Cr1	1.21	4.65	4.76	0.00	0.33	-0.00	0.00	0.10	0.00
Cr2	1.71	4.00	7.99	0.00	-0.10	-0.02	0.02	0.00	0.00
O1	-0.54	-0.48	-3.82	0.00	-0.34	0.00	0.02	-0.01	0.00
O2	-0.78	-3.43	-1.39	-0.47	0.16	-0.20	1.62	-0.07	1.42
O3	-1.06	-0.21	-0.20	0.00	0.01	0.00	0.01	0.10	0.00

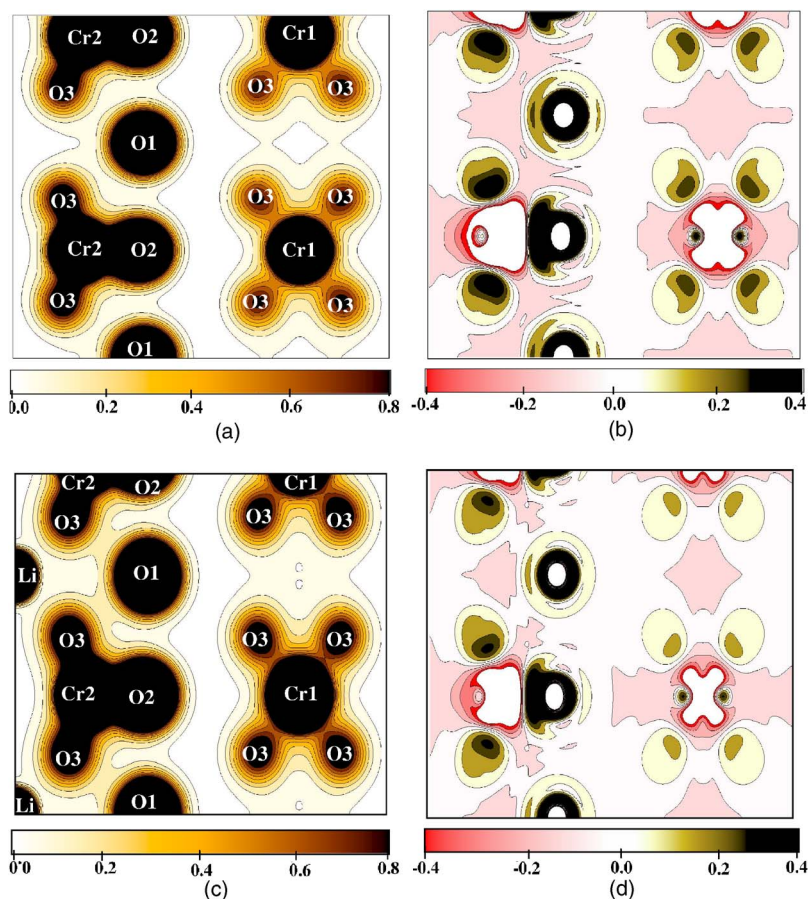


FIG. 6. (Color online) Plots in a, c plane of (a) charge density and (b) charge transfer for Cr_3O_8 -I. Corresponding plots for LiCr_3O_8 -I are shown in (c) and (d), respectively.

diagonal tensor components clearly indicate large covalent contribution to the bonding interactions. Since the calculated BEC values can be considered as upper limits for the formal valence state of a constituent, Li, Cr1, Cr2, O can be assigned $1+$, $3+$, $4+$, and $1.5-$ valence states, respectively. Therefore it would be inappropriate to assign valence states for constituents in such complex oxides according to the conventional approach.

D. Bonding characteristics

The information on the chemical bonding in the compounds under investigation is largely gathered from careful analysis of the structural, magnetic, and DOS properties (Secs. IV A–IV C) together with charge density and charge transfer plots. The insight already gained¹ on the chemical bonding in the closely related compounds ACr_3O_8 ($A = \text{Na, K, Rb}$) constitutes a firm basis for the present deductions. Our very broadly directed study of the ACr_3O_8 compounds included the use of electron localization function and crystal orbital Hamiltonian population analyses as additional tools. However, since the extra tools largely served to confirm the findings from the charge density and charge transfer plots, it was decided to concentrate the efforts on the latter means to illuminate bonding for the present compounds.

In the following we will focus the attention on the bonding situation in Cr_3O_8 -I and LiCr_3O_8 -I. There are two main reasons for this choice. First, LiCr_3O_8 -I is properly isostructural with the ACr_3O_8 compounds which allows us to draw

heavily on the experience from our earlier study¹ and Cr_3O_8 -I constitutes the “anionic” skeleton of these compounds. Second, the Cr_3O_8 -I/ LiCr_3O_8 -I pair are of considerable interest in relation to battery aspects, both for pure model considerations and also for potential practical utilization. Moreover, we believe that insight gained on the bonding in Cr_3O_8 -I and LiCr_3O_8 -I has large carryover value for illustration of our findings for the closely related phases subject to this study.

Figure 6 shows plots of charge density and charge transfer (difference between the actual charge in the crystalline solid under investigation and the superposed atomic charge at the corresponding atomic position) for Cr_3O_8 -I and LiCr_3O_8 -I. The charge density within the Cr_3O_8 -I skeleton [Fig. 6(a)] suggests that the octahedral Cr1 exhibits considerable covalent interaction with the neighboring basal plane oxygen atoms whereas the charge density between Cr2 and oxygen implies even stronger covalent interaction. However, the charge transfer plot [Fig. 6(b)] does not fully comply with these inferences. The anisotropic charge distribution at Cr1 points to coordinated covalent bonding. The absence of charges in regions between Cr2 and O (an indicator for covalent bonding) and more positive charges at the oxygen sites imply that Cr2 exhibits a distinct degree of iono-covalent interaction with its oxygen neighbors (viz. the Cr2-O bonds signal both charge transfer and directional covalent bonding). In LiCr_3O_8 -I [see Figs. 6(c) and 6(d)], the Li site carries charge; the charges around O2 show a somewhat larger span than that in Cr_3O_8 -I, and Cr2-O exhibits

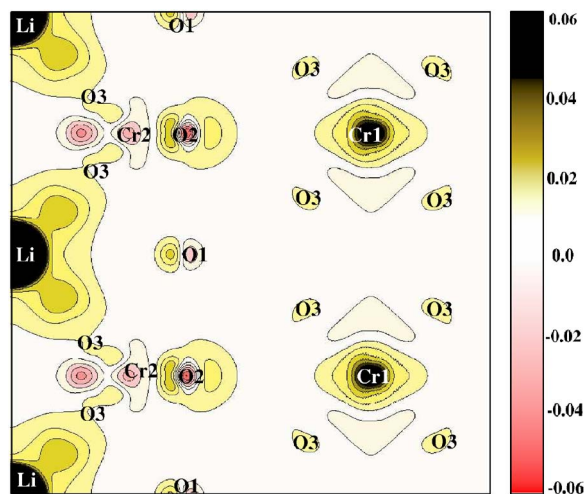


FIG. 7. (Color online) Calculated charge density differences between $\text{LiCr}_3\text{O}_8\text{-I}$ and $\text{Cr}_3\text{O}_8\text{-I}$. The calculations were performed for the fixed, relaxed geometry of $\text{LiCr}_3\text{O}_8\text{-I}$.

higher charge density between the atoms. Except for these distinctions, the overall features of the charge density distribution are the same for $\text{Cr}_3\text{O}_8\text{-I}$ and $\text{LiCr}_3\text{O}_8\text{-I}$.

Similar to Na, K, and Rb in the ACr_3O_8 compounds, it is appropriate to refer to Li in $\text{LiCr}_3\text{O}_8\text{-I}$ as a cation. The same applies to Li in $\text{LiCr}_3\text{O}_8\text{-II}$ although the picture is a little more unclear owing to its more irregular structural arrangements. In $\text{Cr}_3\text{O}_8\text{-I}$ and -II as well as in the lithium containing compounds, Cr and O electronic states are energetically degenerate demonstrating strong covalent interaction between them. The different actual valence states of the Cr atoms in these compounds are seen from their different DOS curves. However, the difference is, in all phases, far smaller than indicated by the formal ionic charges of $3+$ and $6+$. As for the ACr_3O_8 compounds the octahedrally coordinated Cr1 may to a reasonable approximation be regarded as Cr^{3+} whereas the tetrahedrally coordinated Cr2 appears to be closer to Cr^{4+} than Cr^{6+} . The charges associated with oxygen in the presently considered compounds appear close to -1.5 . The general feature is that the Cr-O bonds of octahedral configurations have more covalent character than those in tetrahedral arrangements.

1. Effect of Li intercalation

In order to illustrate the effect of Li intercalation in the $\text{Cr}_3\text{O}_8\text{-I}$ lattice, we show the charge density difference between $\text{LiCr}_3\text{O}_8\text{-I}$ and $\text{Cr}_3\text{O}_8\text{-I}$ in Fig. 7. The charge difference has been calculated for the same unit-cell dimensions and atomic positions as that of the optimized $\text{LiCr}_3\text{O}_8\text{-I}$ phase, so that the electron densities can be subtracted point by point in real space. According to the classic ionic viewpoint: When Li is intercalated into the $\text{Cr}_3\text{O}_8\text{-I}$ host lattice, Cr will absorb the extra charge and change oxidation state(s). If this had been the case, one would have expected appreciable modification in the electronic structure. From Figs. 6(a) and 6(c) it is however seen that there occurs no significant change at the site allocated for Li when it enters the $\text{Cr}_3\text{O}_8\text{-I}$ host to form $\text{LiCr}_3\text{O}_8\text{-I}$, and the amount of charges

present on Cr remains essentially the same. Hence the entire valence electron of Li is not transferred to the $\text{Cr}_3\text{O}_8\text{-I}$ host. Figure 7 suggests that charges are present between the Li and O3 sites. The oxygen electrons are polarized toward the Li site in an “attempt” to establish covalent bonding with Li. In accordance with this, there occurs an increase in the Cr1-O3 bond length from 1.88 \AA in $\text{Cr}_3\text{O}_8\text{-I}$ to 1.91 \AA in $\text{LiCr}_3\text{O}_8\text{-I}$. If the “attempted” Li-O covalent bond had been established as a strong bond, Li deintercalation would have been hampered. However, experimental studies on Cr_3O_8 (unspecified) appears to indicate that the rechargeability and cyclability is quite good, suggesting that the covalency of the Li-O bond is weak. It is worthwhile to note that the O p states span up to E_F in $\text{Cr}_3\text{O}_8\text{-I}$, whereas in $\text{LiCr}_3\text{O}_8\text{-I}$ they become more localized and occur between -6 to -2 eV . Moreover the participation of O p states will give rise to higher cell voltage as more energy is needed to release the electrons from the lower O p band³² during the Li to Li^+ conversion.

As already emphasized, the conventional picture of Li donating its valence electron to the host is not applicable here. The mechanism is rather that the lattice undergoes a “self-regulating response” which minimizes the effect of the external perturbations via rehybridization.⁵ This is seen as noticeable modifications in the charges around Cr and O atoms in Figs. 6(c) and 7. The Cr-O bonds undergo changes in hybridization so that Cr1 gains some charges whereas Cr2 depletes some charges. (The integrated charge at the Cr1 site is $10.42e$ in $\text{Cr}_3\text{O}_8\text{-I}$ and $10.52e$ in $\text{LiCr}_3\text{O}_8\text{-I}$ whereas that at the Cr2 site is $11.64e$ in $\text{Cr}_3\text{O}_8\text{-I}$ and $11.62e$ in $\text{LiCr}_3\text{O}_8\text{-I}$.) A similar situation appears to occur in³³ LiCuSn where the Cu site is mainly affected by the Li intercalation. As the Cr1-O bond length increases from $\text{Cr}_3\text{O}_8\text{-I}$ to $\text{LiCr}_3\text{O}_8\text{-I}$, the strength of the covalent interaction decreases. In general it may be said that the valence electrons on a particular atom participate either in bonding or in magnetism. As the Cr1-O bond length increases, the Cr1 electrons contribute more to magnetism which in turn result in increased magnetic moment at Cr1. The situation for Cr2 is different since the average Cr2-O bond length (1.66 \AA) remains almost the same in $\text{Cr}_3\text{O}_8\text{-I}$ and $\text{LiCr}_3\text{O}_8\text{-I}$, and consequently no noticeable change in either the bonding interaction or the magnetism takes place.

V. CONCLUSION

On considering a number of different guess structures in structural optimizations of Cr_3O_8 and LiCr_3O_8 , it is established that both compounds stabilize with the structural arrangements described in space group $C2/m$ with certain modifications in the atomic arrangements. The optimized structural parameters for Cr_8O_{21} are found to be in good agreement with the available experimental values. From total energy studies it is shown that Cr_8O_{21} is energetically more favorable than different variants of Cr_3O_8 . It is proposed that Cr_3O_8 can be stabilized as a metastable phase when electrochemical conditions are imposed on LiCr_3O_8 . Electronic structures have been explored by investigating total and site-projected density of states and it is confirmed that the elec

tronic structure of LiCr₃O₈ has similarities with the structurally related ACr₃O₈ (A=Na,K,Rb) phases. Detailed analyses of the bonding situation reveal that on intercalation of Li into Cr₃O₈, Li does not donate its valence electron to the Cr₃O₈ host. On the contrary, the Cr₃O₈ host undergoes a so-called self-regulating response by modifying the ionic-covalent character of the Cr-O bonds. In all the studied systems Cr exists in two different valences as evident from differences in magnetic moment and electronic structure details. Cr in octahedral coordination can be referred to as Cr^{III} whereas Cr in tetrahedral configuration should not be considered as Cr^{VI}.

The suitability of Cr₃O₈/LiCr₃O₈ combinations as possible cathode materials has been examined from structural points of view. Owing to their potential significance in this respect, experimental studies on structural and magnetic properties are strongly recommended.

ACKNOWLEDGMENT

The authors are grateful to the Research Council of Norway for financial support and computer time at the Norwegian supercomputer facilities.

*Electronic address: vidya.ravindran@kjemi.uio.no

- ¹R. Vidya, P. Ravindran, P. Vajeeston, H. Fjellvåg, and A. Kjekshus, *Phys. Rev. B* **72**, 014411 (2005).
- ²R. P. Ramasamy, P. Ramadass, B. S. Haran, and B. N. Popov, *J. Power Sources* **124**, 155 (2003).
- ³G. Ceder, M. K. Aydinol, and A. F. Kohan, *Comput. Mater. Sci.* **8**, 161 (1997).
- ⁴M. K. Aydinol, A. F. Kohan, G. Ceder, K. Cho, and J. Joannopoulos, *Phys. Rev. B* **56**, 1354 (1997).
- ⁵C. Wolverton and A. Zunger, *Phys. Rev. Lett.* **81**, 606 (1998).
- ⁶R. Koksang and P. Norby, *Electrochim. Acta* **36**, 727 (1991).
- ⁷D. W. Murphy, P. A. Christian, F. J. Disalvo, and J. N. Carides, *J. Electrochem. Soc.* **126**, 497 (1979).
- ⁸O. Yamamoto, Y. Takeda, R. Kanno, Y. Oyabe, and Y. Shinya, *J. Power Sources* **20**, 151 (1987).
- ⁹H. Laucklnd and S. C. Nijhawan, *Prog. Batteries Sol. Cells* **5**, 61 (1984).
- ¹⁰R. Koksang, D. Fauteux, P. Norby, and K. A. Nielsen, *J. Electrochem. Soc.* **136**, 598 (1989).
- ¹¹J. O. Besenhard and R. Schöllhorn, *J. Electrochem. Soc.* **124**, 968 (1977).
- ¹²Y. Takeda, R. Kanno, T. Tsuji, and O. Yamamoto, *J. Power Sources* **9**, 325 (1983).
- ¹³K.-A. Wilhelmi, *Ark. Kemi* **6**, 131 (1967); *Chem. Commun. (London)* (1966) 437.
- ¹⁴K.-A. Wilhelmi, Doctoral Thesis, University of Stockholm (Stockholm, 1966); *Acta Chem. Scand. (1947-1973)* **22**, 2565 (1968).
- ¹⁵T. A. Hewston and B. L. Chamberland, *J. Magn. Magn. Mater.* **43**, 89 (1984).
- ¹⁶P. Norby, A. N. Christensen, H. Fjellvåg, and M. Nielsen, *J. Solid State Chem.* **94**, 281 (1991).
- ¹⁷P. E. Blöchl, *Phys. Rev. B* **50**, 17953 (1994); G. Kresse and D. Joubert, *ibid.* **59**, 1758 (1999).
- ¹⁸G. Kresse and J. Furthmüller, *Comput. Mater. Sci.* **6**, 15 (1996).
- ¹⁹J. P. Perdew, K. Burke, and Y. Wang, *Phys. Rev. B* **54**, 16533 (1996); J. P. Perdew, K. Burke, and M. Ernzerhof, *Phys. Rev. Lett.* **77**, 3865 (1996).
- ²⁰P. Vinet, J. H. Rose, J. Ferrante, and J. R. Smith, *J. Phys.: Condens. Matter* **1**, 1941 (1989).
- ²¹K.-A. Wilhelmi, *Acta Chem. Scand. (1947-1973)* **12**, 1965 (1958).
- ²²M. J. Saavedra, C. Parada, and E. J. Baran, *J. Phys. Chem. Solids* **57**, 1929 (1996).
- ²³Inorganic Crystal Structure Database, Version 2004.2.
- ²⁴J. S. Stephens and D. W. J. Cruickshank, *Acta Crystallogr.* **B26**, 222 (1970).
- ²⁵A. R. Armstrong and P. G. Bruce, *Nature (London)* **381**, 499 (1996).
- ²⁶Y. Takeda, R. Kanno, T. Tsuji, and O. Yamamoto, *J. Electrochem. Soc.* **131**, 2006 (1984).
- ²⁷P. Arora, D. Zhang, B. N. Popov, and R. E. White, *Electrochem. Solid-State Lett.* **1**, 249 (1998).
- ²⁸D. Zhang, B. N. Popov, Y. M. Podrazhansky, P. Arora, and R. E. White, *J. Power Sources* **83**, 121 (1999).
- ²⁹P. Ravindran and R. Asokamani, *Bull. Mar. Sci.* **20**, 613 (1997).
- ³⁰R. M. Martin, *Phys. Rev. B* **9**, 1998 (1974).
- ³¹R. Pick, M. H. Cohen, and R. M. Martin, *Phys. Rev. B* **1**, 910 (1970).
- ³²Y. Liu, T. Fujiwara, H. Yukawa, and M. Morinaga, *Int. J. Mater. Prod. Technol.* **SPM1**, 89 (2001).
- ³³S. Sharma, L. Fransson, E. Sjöstedt, L. Nordström, B. Johansson, and K. Edström, *J. Electrochem. Soc.* **150**, A330 (2003).